26. Vogler WR, Velez-Garcia E, Weiner RS, et al: A phase III trial comparing idarubicin and daunorubicin in combination with cytarabine in acute myelogenous leukemia: a Southeastern Cancer Study Group Study. J Clin Oncol. 1992;10(7):1103-1111.

27. The AML Collaborative Group: A systematic collaborative overview of randomized trials comparing idarubicin with daunorubicin (or other anthracyclines) as induction therapy for acute myeloid leukaemia. Br J Haematol. 1998;103(1):100-109.

28. Seipelt G, Hofmann W K, Martin H, et al: Comparison of toxicity and outcome in patients with acute myeloid leukemia treated with high-dose cytosine arabinoside consolidation after induction with a regimen containing idarubicin or daunorubicin. Ann Hematol. 1998;76(3-4):145-151.

Table 1. Clinical Characteristics of Randomized Patients

	HiDAC (n = 389)	Multiagent CT (n = 392)	*P* value
Age (year)	46 (15-64)	47 (15-64)	0.697
WBC ($x10^9$/L)	15.6 (0.1-382)	14.9 (0.2-260)	0.323
Karyotype			
Favorable	108	110	0.210
Intermediate	242	256	
Adverse	27	14	
Unknown	12	12	
Induction			
IDR	196	196	0.914
DNR	193	196	
Induction 1cycle (%)	81.0	81.4	0.886

Number indicates the median, and parentheses the range

Table 2. Factors to predict unfavorable prognostic features for DFS and OS by multivariate analysis

a. DFS

variables		hazard ratio	*P* value
Initial WBC Count	>= 20 x 10^9 /L	1.49	<.0001
No of Induction therapies	2 courses	1.50	0.0006
Age	> 50 y.o.	1.33	0.0028
Consolidation therapy	Multiagent CT	1.04	0.7128

b. OS

variables		hazard ratio	*P* value
Age	> 50 y.o.	2.00	<.0001
No of Induction therapies	2 courses	1.58	0.0033
Initial WBC Count	>= 20 x 10^9 /L	1.41	0.0070
MPO-positive blast	< 50 %	1.42	0.0149
Consolidation therapy	Multiagent CT	0.96	0.7768

Table 3. Tolerance of Consolidation

	% receiving the full courses	
	HiDAC	Multiagent CT
All patients	72.5	70.2
Patients ≤ 50yr of age	71.9	69.0
Patients > 50yr of age	73.4	71.9
Reason for not receiving the full courses (No. of Pat.)		
Relapse	18	31
Death	10	8
SCT in 1st CR	31	42
Adverse event*	27	13
Patient refusal	11	5
Unknown	10	19

*$P < 0.05$

Table 4. Intensity of Consolidation

	HiDAC	Multiagent CT	*P* value
After 1st Consolidation			
Lowest WBC (x 10^9/L)	0.17	0.40	< 0.0001
Days WBC < 1.0 x 10^9/L	13	12	0.0005
	(0-40)	(0-36)	
After 2nd Consolidation			
Lowest WBC (x 10^9/L)	0.10	0.40	< 0.0001
Days WBC < 1.0 x 10^9/L	14	13	0.0007
	(0-34)	(0-241)	
After 3rd Consolidation			
Lowest WBC (x 10^9/L)	0.10	0.40	<0.0001
Days WBC < 1.0 x 10^9/L	14	11.5	<0.0001
	(0-38)	(0-28)	
After 4th Consolidation			
Lowest WBC (x 10^9/L)		0.40	
Days WBC < 1.0 x 10^9/L		12	
		(0-34)	

Number indicates the median, and parentheses the range

Table 5. Adverse Events (CTC grades 3 and 4) During Consolidation Therapy

	HiDAC	Multiagent CT	*P*
	%	%	Value
Documented Infection	20.9	14.5	< 0.001
Febrile Neutropenia	66.5	66.4	0.311
Bleeding	0.8	0.7	0.601
Early Death*	0.9	0.6	0.389

Early Death*: death within 30 days after consolidation chemotherapy

Figure Legends

Figure 1: CONSORT diagram

IDR, idarubicin; DNR, daunorubicin; Ara-C, cytarabine, HiDAC, high-dose cytarabine.

Figure 2: Disease-free survival and overall survival according to treatment arm.

a: Disease-free survival of CR patients. Predicted 5-year DFS was 43% for the HiDAC group (n = 389) (red line) and 39% for the Multiagent CT group (n = 392) (blue line) ($P = 0.724$).

b: Overall survival of CR patients. Predicted 5-year OS was 58% for the HiDAC

group (n = 389) (red line) and 56% for the Multiagent CT group (n = 392) (blue line) ($P = 0.954$).

Figure 3: Disease-free survival and overall survival according to treatment arm, after censoring the observation in transplanted patients.

Predicted 5-year DFS was 41% for the HiDAC group (n = 389) (red line) and 36% for the Multiagent CT group (n = 392) (blue line) ($P = 0.608$).

Figure 4: Cumulative incidence of relapse and treatment related mortality in CR by treatment arm.

a: The incidence of relapse and mortality were 49% and 8% for the HiDAC group (solid line), and 56% and 5% for the Multiagent CT group (dotted line) ($P = 0.324$, $P = 0.172$).

b: After censoring the observation in transplanted patients, the incidence of relapse and mortality were 55% and 4% for the HiDAC group (solid line), and 61% and 3% for the Multiagent CT group (dotted line) ($P = 0.402$, $P = 0.409$),

Figure 5: Disease-free survival and overall survival by treatment arm for the favorable cytogenetic risk group.

a: Predicted 5-year DFS was 57% for the HiDAC group (n = 108) (red line) and 39% for the Multiagent CT group (n = 110) (blue line) ($P = 0.050$).

b: Predicted 5-year OS was 75% for the HiDAC group (n = 108) (red line) and 66% for the Multiagent CT group (n = 110) (blue line) ($P = 0.174$).

Figure 6: Disease-free survival and overall survival by treatment arm for the intermediate cytogenetic risk group.

a: Predicted 5-year DFS was 38% for the HiDAC group (n = 242) (red line) and 39% for the Multiagent CT group (n = 256) (blue line) ($P = 0.403$).

b: Predicted 5-year OS was 53% for the HiDAC group (n = 242) (red line) and 54% for the Multiagent CT group (n = 256) (blue line) ($P = 0.482$).

Figure 7: Disease-free survival and overall survival by treatment arm for the

adverse cytogenetic risk group.

a: Predicted 5-year DFS was 33% for the HiDAC group (n = 27) (red line) and 14% for the Multiagent CT group (n = 14) (blue line) ($P = 0.364$).

b: Predicted 5-year OS was 39% for the HiDAC group (n = 27) (red line) and 21% for the Multiagent CT group (n = 14) (blue line) ($P = 0.379$).

Fig 1

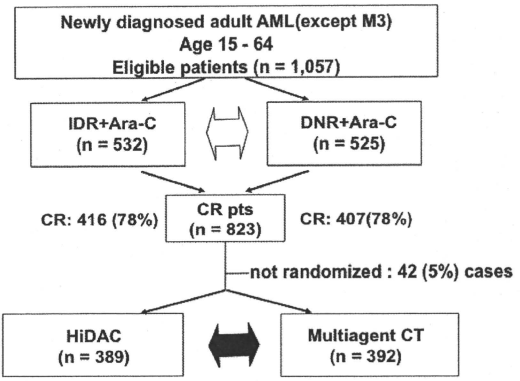

Fig 2

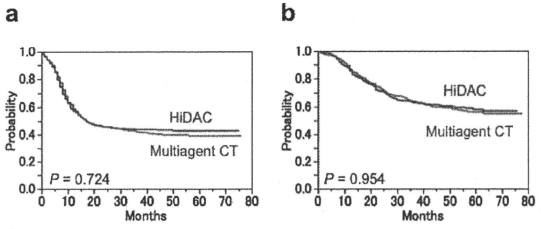

Fig 3

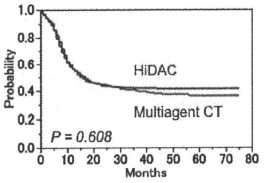

Fig 4

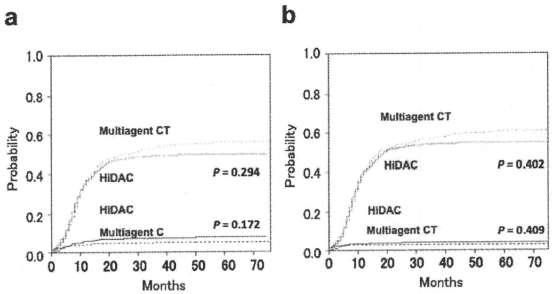

Fig 5

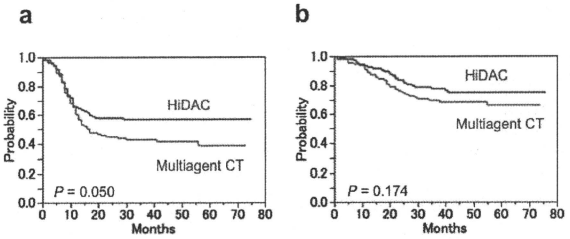

Fig 6

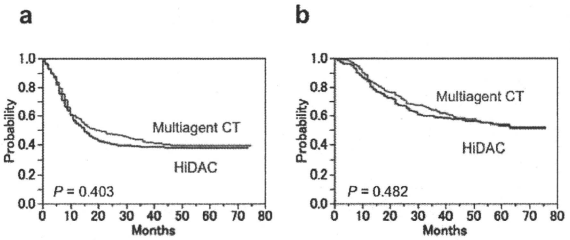

Fig 7

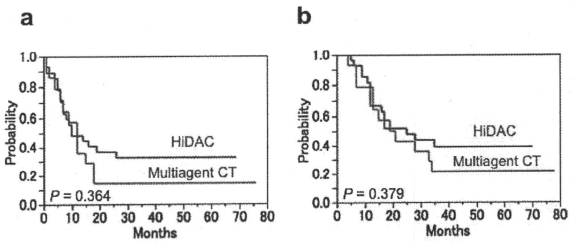

Open

Leukemia (2011), 1–13

www.nature.com/leu

ORIGINAL ARTICLE

LBH589, a deacetylase inhibitor, induces apoptosis in adult T-cell leukemia/lymphoma cells via activation of a novel RAIDD-caspase-2 pathway

H Hasegawa[1], Y Yamada[1], K Tsukasaki[2], N Mori[3], K Tsuruda[1], D Sasaki[1], T Usui[1], A Osaka[1], S Atogami[1], C Ishikawa[3,4], Y Machijima[3], S Sawada[3], T Hayashi[5], Y Miyazaki[2] and S Kamihira[1]

[1]*Department of Laboratory Medicine, Nagasaki University Graduate School of Biomedical Sciences, Nagasaki, Japan;* [2]*Department of Hematology, Atomic Disease Institute, Nagasaki University Graduate School of Biomedical Sciences, Nagasaki, Japan;* [3]*Division of Molecular Virology and Oncology, Graduate School of Medicine, University of the Ryukyus, Nishihara, Okinawa, Japan;* [4]*Transdisciplinary Research Organization Subtropics Island Studies, University of the Ryukyus, Nishihara, Okinawa, Japan and* [5]*Department of Pathology, Nagasaki University Hospital, Nagasaki, Japan*

Adult T-cell leukemia/lymphoma (ATLL), an aggressive neoplasm etiologically associated with human T-lymphotropic virus type-1 (HTLV-1), is resistant to treatment. In this study, we examined the effects of a new inhibitor of deacetylase enzymes, LBH589, on ATLL cells. LBH589 effectively induced apoptosis in ATLL-related cell lines and primary ATLL cells and reduced the size of tumors inoculated in SCID mice. Analyses, including with a DNA microarray, revealed that neither death receptors nor p53 pathways contributed to the apoptosis. Instead, LBH589 activated an intrinsic pathway through the activation of caspase-2. Furthermore, small interfering RNA experiments targeting caspase-2, caspase-9, RAIDD, p53-induced protein with a death domain (PIDD) and RIPK1 (RIP) indicated that activation of RAIDD is crucial and an event initiating this pathway. In addition, LBH589 caused a marked decrease in levels of factors involved in ATLL cell proliferation and invasion such as CCR4, IL-2R and HTLV-1 HBZ-SI, a spliced form of the HTLV-1 basic zipper factor HBZ. In conclusion, we showed that LBH589 is a strong inducer of apoptosis in ATLL cells and uncovered a novel apoptotic pathway initiated by activation of RAIDD.
Leukemia advance online publication, 18 January 2011;
doi:10.1038/leu.2010.315
Keywords: LBH589; apoptosis; adult T-cell leukemia; caspase-2; RAIDD

Introduction

There is evidence that gene expression governed by epigenetic changes is crucial to the pathogenesis of cancer.[1] Histone deacetylases are enzymes involved in the remodeling of chromatin, and have a key role in the epigenetic regulation of gene expression. In addition, the activity of non-histone proteins can be regulated through histone deacetylase-mediated hypoacetylation.[2] Deacetylase inhibitors (DACi) induce the hyperacetylation of non-histone proteins, as well as nucleosomal histones resulting in the expression of repressed genes involved in growth arrest, terminal differentiation and/or apoptosis among cancer cells.[3,4] Several classes of DACi have been found to have potent anticancer effects in preclinical studies.[2] Despite a consensus on the importance of apoptosis to the effect of these drugs, different apoptotic mechanisms have been reported.[2] For instance, even the contribution of caspases to DACi-induced apoptosis is quite controversial.[5–8]

Correspondence: Dr Y Yamada, Department of Laboratory Medicine, Nagasaki University Graduate School of Biomedical Sciences, 1-7-1 Sakamoto, Nagasaki City 852-8501, Japan.
E-mail: y-yamada@nagasaki-u.ac.jp
Received 1 April 2010; revised 24 November 2010; accepted 10 December 2010

There are two general apoptotic pathways, the receptor (extrinsic) pathway and the mitochondrial (intrinsic) pathway.[9] The extrinsic pathway requires activation of caspase-8, which results in activation of the zymogens of executioner caspases such as caspase-3, eventually leading to cleavage of poly ADP-ribose polymerase (PARP). Proteolytic caspase-8 can further activate BH3-interacting domain death agonist (BID), and cleaved BID moves to the mitochondria where it triggers the release of cytochrome-*C*. In the intrinsic pathway, death signals lead to changes in the mitochondrial outer membrane's permeability, subsequently releasing cytochrome-*C*, which forms an apoptosome with caspase-9, eventually activating executioner caspases.[10]

LAQ824 and the more potent and newly developed DACi analog LBH589 are now under clinical investigation as a therapeutic agent for several kinds of cancer.[2,4] One unique feature of these drugs is their role in the regulation of heat shock protein 90kDa-α (HSP90) and degradation of HSP90 client proteins such as bcr–abl in chronic myelogenous leukemia and fms-related tyrosine kinase 3 in acute myeloid leukemia.[11–15]

Adult T-cell leukemia/lymphoma (ATLL) is a neoplasm of mature T-lymphocyte origin etiologically associated with human T-lymphotropic virus type-1 (HTLV-1) and is known to be resistant to standard anticancer therapies.[16] Previous findings suggest that the viral protein HTLV-1 Tax interferes with most DNA repair mechanisms, preventing cell cycle arrest and apoptosis, and contributing to the early stages of ATLL.[17,18] In addition, the novel viral protein HTLV-1 basic zipper factor (HBZ) and its spliced form (HBZ SP1RNA or HBZ-SI), which are encoded by the minus-strand RNA of the HTLV-1 genome, have been identified recently.[19–23] These proteins are thought to be functional and expected to be closely involved in the late stages of ATLL.[24] ATLL is generally classified into four clinical subtypes: acute, chronic, smoldering and lymphoma. Although several approaches have been reported, combination chemotherapy is still the treatment of choice for newly diagnosed acute and lymphoma-type ATLL. Patients with aggressive ATLL have a median survival period of 13 months, indicating limitations in the treatment of ATLL.[25,26] In this study, we examined the effects of LBH589 on ATLL cells *in vitro* and *in vivo*, and investigated the pathways or factors contributing to the LBH589-induced ATLL cell death.

Materials and methods

Cell preparation

The ATLL-derived cell lines ST1, KOB, LM-Y1, LM-Y2, KK1 and SO4 were established in our laboratory from ATLL patients[27,28] and maintained in RPMI 1640 medium supplemented with

10% fetal bovine serum and 0.5 U/ml of interleukin-2 (kindly provided by Takeda Pharmaceutical Company, Ltd., Osaka, Japan). The HTLV-1-infected T-cell lines MT2 and HuT102,[29,30] human T-cell leukemia cell line Jurkat and erythromyeloblastoid cell line K562 were maintained in RPMI 1640 medium supplemented with 10% fetal bovine serum. The ST1, KOB, LM-Y1, MT2 and HuT102 cells have the wild-type p53.[31] Primary leukemia cells from eight patients with acute-type ATLL were also analyzed. The diagnosis of ATLL and preparation of peripheral blood mononuclear cells from patients with ATLL and normal healthy donors were described previously.[28] Each patient's sample contained more than 80% leukemia cells at the time of analysis. After approval by the Ethics Committee at Nagasaki University Hospital, all materials from patients were obtained with informed consent.

Chemicals and cell proliferation assay

Chemicals used in this study were LBH589 (kindly provided by Novartis Pharma AG., Basel, Switzerland), SAHA (Cayman Chemical, Ann Arbor, MI, USA), MG132 (Biomol Research Laboratories, Plymouth Meeting, PA, USA), LY294002 (Biomol), soluble tumor necrosis factor related apoptosis-inducing ligand (TRAIL) (Biomol), staurosporine (Merck, Darmstadt, Germany), the pan-caspase inhibitor z-VAD-fmk, the caspase-2 inhibitor Z-VDVAD-fmk and the caspase-9 inhibitor Z-LEHD (MBL, Nagoya, Japan). The cell proliferation assay (3-(4,5-dimethylthiazol-2-yl)-5-(3-carboxymethoxyphenyl)-2-(4-sulfophenyl)-2H-tetrazolium, inner salt assay) was performed with a Cell Titer 96 AQueos Cell Proliferation Assay kit (Promega, Madison, WI, USA) according to the manufacturer's directions.

In vivo *experiments using SCID mice*

Five-week-old female C.B-17/Icr-SCID mice obtained from Ryukyu Biotec (Urasoe, Japan) were maintained in containment level 2 cabinets and provided with autoclaved food and water *ad libitum*. The mice were engrafted with 10^7 HuT102 cells by subcutaneous injection in the post-auricular region and randomly placed into two cohorts of five animals each that received vehicle or LBH589. Treatment was initiated on the day after cell injection. LBH589 was dissolved in distilled water at a concentration of 2 mg/ml, and 28 mg/kg body weight of LBH589 was administered by oral gavage three times a week. Control mice received the same volume of the vehicle only. Body weight and tumor numbers and size were monitored once a week. All mice were sacrificed on day 28, then the tumors were dissected out, and their weight was measured. After tumors were fixed for paraffin embedding and tissue sectioning, DNA fragmentation was evaluated by fluorescent TUNEL (TAKARA BIO INC., Shiga, Japan) as recommended by the manufacturer. All these experiments were performed according to the Guidelines for Animal Experimentation of the University of the Ryukyus and were approved by the Animal Care and Use Committee of the same university.

Flow cytometric analysis

To evaluate apoptotic changes and the permeability of the mitochondrial outer membrane, we used an Annexin-V and PI Kit (Bender Medsystems, Vienna, Austria) and a Mitochondrial Membrane Potential Assay Kit (5, 5′, 6, 6′-tetrachloro-1, 1′, 3, 3′-tetraethylbenzimidazol-carbocyanine iodide detection) (Cayman Chemical), respectively. Activities of caspase-8 and 9 were determined by fluorometric assay (MBL) according to the manufacturer's instructions. The cell-surface expression of death receptors (DRs), CCR4 and IL-2R was examined by flow cytometric analysis using anti-tumor necrosis factor-R1 (MBL), anti-CD95 (BD Biosciences, San Diego, CA, USA), anti-DR5 (Alexis Biochemicals, San Diego, CA, USA), anti-CCR4 (BD) and anti-CD25 (BD) monoclonal antibodies. Mouse IgG1 (DAKO, Kyoto, Japan) was used as a negative control. All experiments were performed using a FACSCalibur flowcytometer and Cellquest software (BD).

Preparation of whole-cell lysate, nuclear, mitochondrial and cytosolic fractions

Cells were harvested after treatment and whole-cell lysate was prepared as described previously.[32] Nuclear extracts from cells were prepared for NF-κB transcription assays using a nuclear/cytosol fractionation kit (BioVision, San Diego, CA, USA), according to the instructions. Similarly, cytosolic fractions were prepared for western blotting by using a mitochondria/cytosol fractionation kit (BioVision).

Western blotting, immunoprecipitation and antibodies

Western blotting was performed as described previously.[31] The analysis was performed using antibodies to p53 (DO-1), MDM2 (Ab-1), FADD, PUMA and NOXA (Merck), phospho-AKT, AKT, caspase-8, 9 and 3, cleaved caspase-9, cleaved PARP, BID, BAX, Bcl-xL, cytochrome-c, p21 and acetylated-Lysin (Cell Signaling Technology, Beverly, MA, USA), p53-induced protein with a death domain (PIDD) (LifeSpan Biosciences, Seattle, WA, USA), caspase-2 (11B4) and c-FLIP (Dave-2) (Alexis), RAIDD and TRADD (MBL), survivin (R&D systems Inc., Minneapolis, MN, USA), acetylated-histone-H3 and -H4, and Bcl-2 (Upstate Biotechnology, Waltham, MA, USA), RIP and XIAP (BD), HBZ (kindly provided by Dr JM Mesnard) and HBZ-SI,[22] Tax,[31] acetylated-tubulin, α-tubulin and β-actin (Sigma Chemicals, St Louis, MO, USA). In the immunoprecipitation assay, protein A-Sepharose beads (Sigma), HSP90 antibody (StressGen Biotechnologies Corporation, Victoria, BC, Canada) and RAIDD antibody (LifeSpan Biosciences) were used.

Immunohistochemistry

After tumors were fixed for paraffin embedding and tissue sectioning, immunohistochemical staining for acetylated-histone-H3 and -H4 was performed. The deparaffinized slides were pretreated with DAKO Target Retrival Solution (pH 9) (DAKO), and heated in a water bath at 95 °C for 40 min. For all stains, the endogenous peroxidase was quenched by 3% H_2O_2 for 15 min. Sections were then placed in 0.5% nonfat dry milk for 30 min at room temperature. The primary antibodies used were anti-acetylated-histone-H3 and -H4 (Cell Signaling). They were allowed to react for 1 h at room temperature, and then the DAKO EnVision + Dual Link System-HRP (DAKO) was applied using diaminobenzidine as the chromogen, following the manufacturer's directions.

Proteasome activity assay

The proteolytic activity of the 20S proteasome was evaluated with the Biomol AK-740 QuantiZyme Assay System (Biomol) following the manufacturers' instructions, which detects the release of the free 7-amino-4-methylcoumarin fluorophore, upon cleavage of the fluorogenic peptide Suc-LLVYAMC.

DNA microarray analysis

Total RNA from cells was extracted using ISOGEN (Nippon Gene, Toyama, Japan) and purified with a Message Clean kit

(GenHunter Corp., Brookline, MA, USA). The RNA's integrity was assessed using an Agilent 2100 Bioanalyzer (Agilent, Palo Alto, CA, USA). Double-stranded cDNA and biotinylated cRNA were synthesized using a T7-poly-T primer and the BioArray RNA labeling kit (Enzo, Farmingdale, NY, USA), respectively. The labeled RNA was then fragmented and hybridized to HU-133A oligonucleotide arrays (Affymetrix, Santa Clara, CA, USA). The arrays were scanned using the Gene Array Scanner and analyzed using the DNA-Chip Analyzer.

Real-time quantitative RT-PCR

After total RNA was prepared as described above, Real-time RT-PCR for HBZ, HBZ-SI and Tax were performed using a LightCycler Technology System (Roche Diagnostics, Basel, Switzerland) as described previously.[22,28,33] Similarly, PCRs for caspase-2, caspase-9, RAIDD, PIDD and PBGD were performed on a Roche LC480 (Roche) with LightCycler 480 Probes Master mix (Roche) according to the directions. We designed specific sets of primers and/or purchased probes as summarized in Supplementary Table 1.

NF-κB transcription factor assay

Nuclear extracts from cells were prepared as described above. Activities of NF-κB p50 and p65 were investigated using an NF-κB transcription factor assay kit (Chemicon, Temecula, CA, USA) as recommended by the manufacturer.

Transfection, luciferase assay and small interfering RNA experiments

Transfection was performed with a Cell line Nucleofector kit V and the Nucleofector system (Lonza, Cologne, Germany). The transfection programs for ST1 (O-17) and HuT102 (O-16) were determined so that the viability of cells and the transfection efficiency would be compatible (data not shown). Luciferase assays using reporter plasmid pG13-Luc were described previously.[31] The plasmid Myr-AKT (pcDNA3 myr-HA-Akt1) was obtained from Addgene Inc. (Cambridge, MA, USA).[34] Empty pcDNA3 or Myr-AKT vectors were used for the AKT-transfection experiment. Cells (5×10^6) were resuspended in 100 μl of Cell line Nucleofector solution V and mixed with 2 μg of plasmid DNA. Twenty-four hours after transfection, the cells were cultured with or without LBH589 and processed for flow cytometric analysis or western blotting. We prepared three different small interfering RNA (siRNA) against each target. Caspase-2: Silencer Select Validated siRNA s2412 (#1), s2410 (#2) and s2411 (#3), caspase-9: Silencer Select siRNA s2430 (#1), s2428 (#2) and s2429 (#3), RAIDD: Silencer Select siRNA s16656 (#1), s16654 (#2) and s16655 (#3), PIDD: Silencer Select siRNA s30843 (#1), s30844 (#2) and s226845 (#3), RIP: Silencer Select Validated siRNA s16651 (#1), s11652 (#2) and s16653 (#3), and control siRNA (Silencer negative control #1) (Applied Biosystems, Foster City, CA, USA). After evaluating the effect of each siRNA by monitoring the target's mRNA and protein (Supplementary Figure 2), we eventually selected a set of #1 siRNA against each target. Cells were used 24 h after transfection and each siRNA experiment was performed in triplicate.

Results

LBH589 causes acetylation of histones and non-histone proteins in ATLL cells

Hydroxamate-based DACi including LBH589 induce hyperacetylation of histones H3/H4 and α-tubulin.[2,4] Recent reports also indicated that LAQ824 and LBH589 can cause acetylation of HSP90 and the disruption of its chaperone function, resulting in repression of HSP90 client proteins including AKT.[12,35] We first confirmed that LBH589 was very effective in increasing the acetylation of histones H3/H4 and α-tubulin in ATLL-related cell lines (Figure 1a). As expected, LBH589 also caused acetylation of HSP90 in ST1, KOB and KK1 cells and significantly reduced the expression of phospho-AKT (Figures 1b and c).

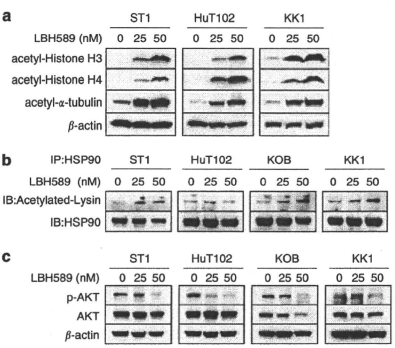

Figure 1 LBH589 causes acetylation of histones and non-histone proteins in adult T-cell leukemia/lymphoma (ATLL) cells. Cells were treated with either vehicle or the indicated concentrations of LBH589 for 24 h. Whole-cell lysate was prepared, and (**a** and **c**) western blotting was performed. (**b**) For each sample, 100 μg of cell lysate was used for immunoprecipitation with a monoclonal antibody to heat shock protein 90kDa α (HSP-90), and western blotting was performed.

LBH589 induces apoptosis in ATLL cells

Next, we examined the effect of LBH589 on the growth of 8 ATLL-related cell lines, Jurkat cells and K562 cells. LBH589 caused ~60% inhibition of cell growth at a concentration of 25 nM in the ATLL-related cell lines and Jurkat cells, and about 30% inhibition in the K562 cells (Figure 2a). ST1, HuT102 and MT2 cells were especially sensitive with more than 60% of their growth inhibited at 12 nM. To determine the details of LBH589-mediated cell death, we performed Annexin-V/PI staining. After 48-h treatment with 25 nM of LBH589, Annexin-V-positive cells in the ST1 and HuT102 cell lines increased from 8 and 4% to 71 and 92%, respectively (Figure 2b). Likewise, more than 30% of cells were positive for Annexin-V after 24-h treatment with 25 nM of LBH589 in the other cell lines except K562, in which the proportion was 9.5% (Figure 2c). These results indicate that ATLL-related cell lines are highly sensitive to LBH589-induced apoptosis. Similar to the results for the cell lines, LBH589 significantly inhibited cell proliferation in all primary ATLL cell samples examined. In contrast, normal peripheral blood mononuclear cells were less harmed than ATLL cells (Figure 2d). Annexin-V/PI staining confirmed that LBH589 induces apoptotic cell death in primary ATLL cell samples (Figure 2e).

Treatment of subcutaneous tumors with LBH589

We examined whether LBH589 is also effective against ATLL cells in the *in vivo* setting, by using SCID mice transplanted with HuT102 cells. Ten mice were inoculated, five of which were

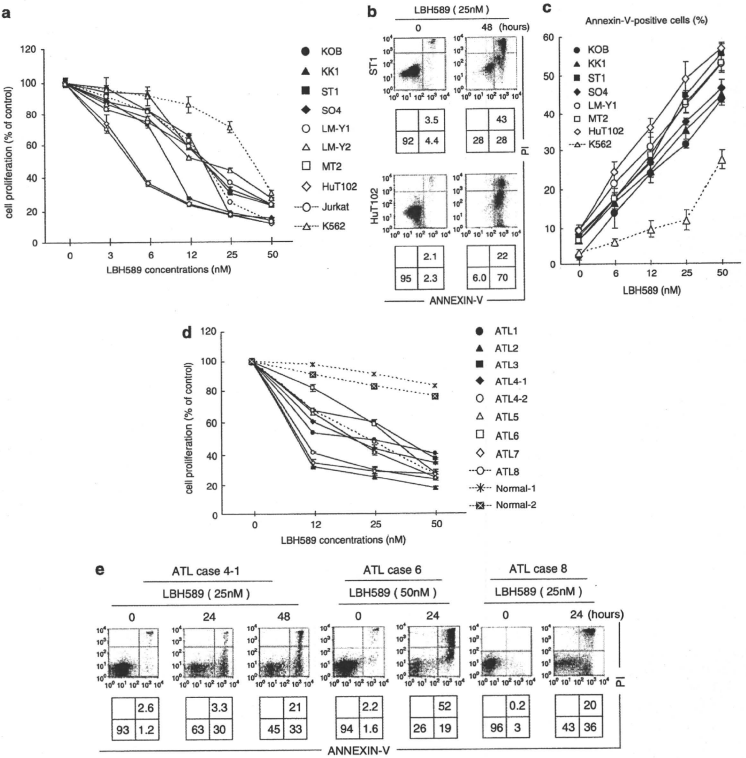

Figure 2 LBH589 induces apoptosis in adult T-cell leukemia/lymphoma (ATLL)-related cell lines and primary ATLL cells. (**a** and **d**) Cell lines ($3–5 \times 10^5$/ml), primary ATLL cells or normal peripheral blood mononuclear cell (PBMCs) ($7–10 \times 10^5$/ml) were treated with either vehicle or the indicated concentrations of LBH589 for 48 h and cell proliferation (% against cells cultured without LBH589) was evaluated by MTS (3-(4, 5-dimethylthiazol-2-yl)-5-(3-carboxymethoxyphenyl)-2-(4-sulfophenyl)-2H-tetrazolium, inner salt) assay. (**b**, **c** and **e**) After cells were treated with the indicated concentrations and time course, Annexin-V/PI staining was performed. (**b** and **e**) Percentages of intact cells (Annexin-V^- PI^-), early apoptotic cells (Annexin-V^+ PI^-) and late apoptotic or necrotic cells (Annexin-V^+ PI^+) are indicated in the lower panels. (c) Percentages of Annexin-V-positive cells were evaluated. (**a**, **c** and **d**) Experiments were performed in triplicate and results were expressed as the mean ± s.d. In ATLL case 4, samples from peripheral blood mononuclear cells (4–1) and pleural effusion (4–2) were investigated.

treated with LBH589 and five of which were left untreated. LBH589 reduced the volume of tumors more than 70% (Figure 3a). The mean tumor weight of LBH589-treated mice was significantly lower than that of control mice (Figure 3b). Immunohistochemical staining confirmed that LBH589 was very effective in increasing the acetylation of histones H3/H4 in tumors of treated mice (Figure 3c). We further confirmed by a TUNEL assay that LBH589 caused evident apoptosis in transplanted tumors (Figure 3d).

Analysis of the extrinsic pathway in LBH589-induced apoptosis

DACi are reported to activate the extrinsic pathway, in many cases, in cooperation with (DRs).[2] Among typical DRs, DR5 was expressed in ATLL-related cell lines[28] but tumor necrosis factor-R1 .mostly was not (not shown) and there was no change after LBH589 treatment (not shown). LBH589 rather reduced Fas expression in ST1, LMY1 and HuT102 cells (Figure 4a). In typical DR-mediated apoptosis (Jurkat + TRAIL), both extrinsic and intrinsic pathways are activated including cleavage of BID, which was not observed in K562 cells treated with 12 nM of LBH589 (Figure 4c). In ATLL cell lines, western blotting revealed no bands of cleaved caspase-8 on treatment with LBH589 (Figure 4b). This was accompanied by slight changes in FADD and BID expression (Figure 4b). In contrast, LBH589 reduced the expression of FLIP proteins in HuT102 and KK1 cells (Figure 4b). Fluorometric analysis eventually showed that LBH589 little

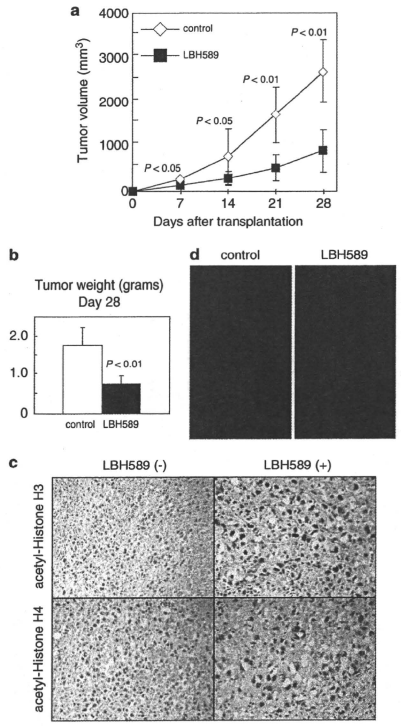

Figure 3 LBH589 reduces tumors inoculated in SCID mice. HuT102 cells (10^7 per mouse) were injected subcutaneously into SCID mice. The mice (five per group) were treated with either vehicle or LBH589. Treatment was initiated on the day after inoculation. Tumor volume and weight were monitored on the indicated days after the injection of cells. (**a**) Serial changes in tumor volume in treated and untreated mice. Data are the mean ± s.d. for five mice each. Mann–Whitney's *U*-test was used to compare results with control values. (**b**) Tumors removed from untreated mice and LBH589-treated mice on day 28 after cell inoculation were weighed. (**c**) Immunohistochemical staining shows the acetylation of histones H3/H4 in tumors of treated mice. (**d**) TUNEL assays show apoptotic cells in tumors from mice treated with LBH589 compared with the control mice. Magnification, × 40.

activated caspase-8 in ATLL-related cell lines in contrast to caspase-9 (Figure 4d). These results suggest that LBH589 does not activate the extrinsic pathway in ATLL-related cell lines.

LBH589 induces apoptosis in ATLL cells by activating the intrinsic pathway

Next, we investigated the changes in permeability of the mitochondrial membrane in cells treated with LBH589 by using the 5, 5′, 6, 6′-tetrachloro-1, 1′, 3, 3′-tetraethylbenzimidazolcarbocyanine iodide dye. The percentage of cells with decreased red fluorescence was increased from 7.3 to 81% and from 11 to 76% in ST1 and HuT102 cells, respectively (Figure 4e). Time course analyses of these changes are shown in Figure 4f. Furthermore, the release of cytochrome-*c* from mitochondria to the cytosol was detected by western blotting (Figure 4g). The activation of caspase-9 was confirmed by the appearance of cleaved caspase-9 and by a fluorometric analysis, which showed a three–eightfold increase after treatment with LBH589 (Figures 4b and d). The bands of cleaved caspase-3 and cleaved PARP, as a result of apoptosis, were clearly observed (Figure 4b). Collectively, these results suggest that the major mechanism of LBH589-induced apoptosis is activation of the intrinsic pathway.

Contribution of caspase-9 and/or AKT in LBH589-induced apoptosis

Interestingly, the band for pro-caspase-9 did not decrease in intensity in spite of its consumption but rather increased on treatment with LBH589 (Figure 4b). AKT has been shown to downregulate the expression of caspase-9 via direct phosphorylation[36] and LBH589 significantly reduced the expression of phospho-AKT (Figure 1c). Then, we used a typical PI3K/AKT inhibitor, LY294002, to investigate the impact of AKT's inactivation in LBH-induced apoptosis. ATLL cell lines with phospho-AKT actually underwent apoptosis and showed a decrease in phospho-AKT on treatment with LY294002. In this setting, however, the expression of caspase-9 was not upregulated (not shown). Furthermore, we performed transfection experiments with myr-AKT. The expression levels of phospho-AKT were not decreased by LBH589 in myr-AKT-transfected HuT102 cells (Supplementary Figure 1B). In this setting, we found that the percentage of Annexin-V-positive cells was decreased in myr-AKT cells (Supplementary Figure 1A). Expression levels of cleaved caspase-3 in LBH589-treated myr-AKT cells were moderately lower than those in mock-transfected cells (Supplementary Figure 1B). However, expression levels of other key molecules including caspase-9 were not altered (Supplementary Figure 1B). These results suggest that the LBH589-induced decrease in phospho-Akt levels is not an event upstream of the LBH589-induced accumulation of caspase-9 but partly contributes to the pro-apoptotic effects of LBH589.

Microarray analysis

We performed a DNA microarray analysis using HuT102 and LM-Y1 cells and compared gene expression profiles between cells treated with LBH589 and cells left untreated focusing on how the intrinsic pathway is activated during LBH589-induced apoptosis (Table 1). Among commonly observed changes, an upregulation of cytochrome-*c* expression and a downregulation of p53 expression were remarkable. An upregulation of caspase-9 expression and a downregulation of FAS expression, were in accord with results of western blotting and flow cytometric analysis, respectively (Figures 4a and b). Taking into consideration the results of the microarray analysis, we performed further studies focusing on three different groups; ATLL-characteristic, p53-related and caspase-2-related proteins.

Analysis of proteins characteristic of ATLL cells

We first focused on CCR4 and IL-2R, which were remarkably affected by LBH589 (Table 1). A majority of ATLL cells

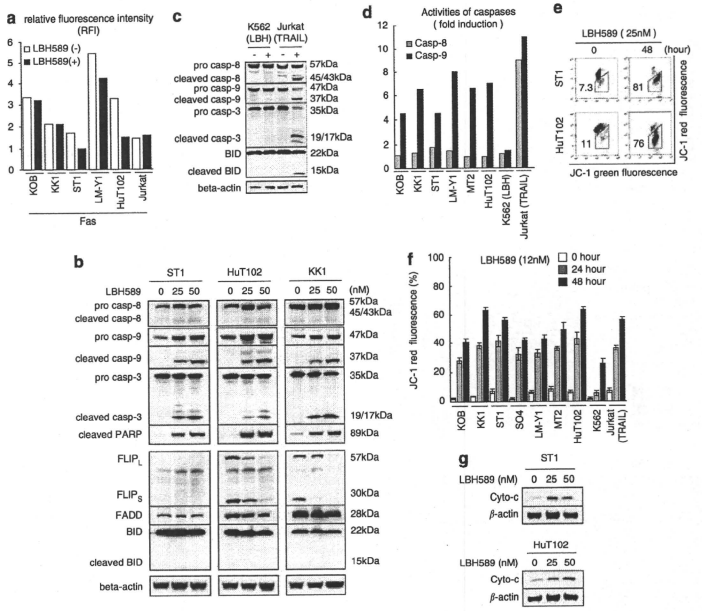

Figure 4 Analysis of the apoptotic pathway in LBH589-induced cell death. Cells were treated with either vehicle or the indicated concentrations of LBH589 for 24–48 h. After cells were harvested, flow cytometric analysis (FCM) (**a**, **d**, **e** and **f**) or western blotting (**b** and **g**) was performed. Tumor necrosis factor-related apoptosis-inducing ligand (TRAIL) (100 ng/ml)-treated Jurkat cells were used as a positive control of typical apoptosis and LBH589 (12 nM)-treated K562 cells were used as a negative control (**c**, **d** and **f**). (**a**) Changes in expression of Fas were indicated using RFI (the ratio of mean fluorescence intensity for specific staining to that for control staining). (**d**) Activities of caspases. Cells were incubated with the IETD-FMK for caspase-8, conjugated to FITC (FITC-IETD-FMK) or the LEHD-FMK for caspase-9, conjugated to FITC (FITC-LEHD-FMK) and analyzed using FCM. Comparison of the fluorescence intensity in the treated sample with that of the untreated control allows determination of the fold increase in activity of each caspase. (**e** and **f**) Mitochondrial membrane permeability. Cells were incubated with the JC-1 dye and analyzed using FCM. The percentage of cells with low JC-1 red fluorescence was evaluated. (**b**, **c** and **g**) Western blotting was performed using whole-cell lysate (**b** and **c**) or a cytosolic fraction (**g**) prepared as described in Materials and methods.

consistently express CCR4, which contributes to tumor cell progression and/or invasion.[37] ATLL-related cell lines had high levels of CCR4, which were dramatically decreased by LBH589 treatment (Figure 5a). IL-2R is also known to be overexpressed in ATLL cells and is often used as a diagnostic marker for ATLL.[17] LBH589 repressed the expression of IL-2R ~50% in the ATLL-related cell lines though levels were still extremely high (Figure 5b). Importantly, IL-2R is a typical gene whose promoter is activated by HTLV-1 Tax. Then, we investigated whether the expression of Tax mRNA is also affected by LBH589. The effect depended on the cells examined. In cells with high Tax mRNA levels (KOB, MT2 and HuT102), the expression tended to increase with LBH589 treatment, while in cells with relatively low Tax mRNA levels (LMY1, KK1 ST1 and SO4), it tended to decrease (Figure 5c). These results were consistent with those of western blotting (Figure 5c upper panel). The behavior of the HBZ mRNA was similar to that of the Tax mRNA; cells with high Tax levels tended to show an increase in HBZ mRNA on LBH589 treatment, while cells with lower Tax levels tended to exhibit a decrease (Figure 5d). In contrast, LBH589 significantly repressed HBZ-SI mRNA expression in ATLL-related cell lines except MT2 cells (Figure 5e). Protein levels of HBZ and HBZ-SI were not high in any cells examined and the expression profiles were approximately the same as those for the mRNA (Figures 5d and e). As NF-κB is constitutively activated in ATLL cells dependent on and/or independent of HTLV-1 Tax[38,39] and the repression of NF-κB is an important mechanism in DACi-induced ATLL cell death,[40,41] we examined the activities of NF-κB. However, repression of NF-κB by LBH589 was not commonly observed in ATLL-related cell lines (not shown).

LBH589-induced apoptosis in ATLL cells does not depend on the p53 pathway

Although p53 is an important inducer of the intrinsic apoptotic pathway, its gene expression was significantly decreased by LBH589 treatment (Table 1). To verify this phenomenon, we performed a luciferase assay with pG13-Luc using ST1, HuT102, KOB and KK1 cells and found that activation of p53 had not occurred (not shown). Unexpectedly, LBH589 reduced the

Table 1 Microarray analysis of HuT102 cells

Symbol	*Gene*	*Fold change*	
		HuT102	*LM-Y1*
SPP1	Secreted phosphoprotein 1 (osteopontin, bone sialoprotein I, early T-lymphocyte activation-1)	6.4	9.4
DHRS2	Dehydrogenase/reductase (SDR family) member-2	6.2	2.5
SERPINB2	Serpin peptidase inhibitor, clade B (ovalbumin), member-2	5.6	3.8
CASP9	Caspase 9, apoptosis-related cysteine peptidase	3.9	1.7
BTG2	BTG family, member-2	3.4	2.2
CYCS	Cytochrome-*c*, somatic	3.4	2.1
CLU	Clusterin	3.1	2.1
CTSB	Cathepsin B	3.1	3.5
GADD45B	Growth arrest and DNA damage inducible, beta	2.9	3.6
PHLDA1	Pleckstrin homology-like domain, family A, member-1	2.9	2.0
EFHC1	EF-hand domain (C-terminal) containing 1	2.8	2.6
IFI6	Interferon, alpha-inducible protein 6	2.7	2.2
NLRP1	NLR family, pyrin domain containing 1	2.7	1.1
LOH11CR2A	Loss of heterozygosity, 11, chromosomal region 2, gene A	2.6	2.3
RARRES3	Retinoic acid receptor responder (tazarotene induced) 3	2.5	2.5
ARHGAP20	Rho GTPase activating protein 20	2.3	1.7
BCL10	B-cell CLL/lymphoma 10	2.3	1.5
BTG1	B-cell translocation gene 1, anti-proliferative	2.3	1.4
ACVR1C	Activin A receptor, type IC	2.2	1.0
FASLG	Fas ligand (TNF superfamily, member-6)	2.2	—
RECK	Reversion-inducing-cysteine-rich protein with kazal motifs	2.2	—
SIAH2	Seven in absentia homolog 2 (*Drosophila*)	2.2	—
APAF1	Apoptotic peptidase-activating factor-1	2.1	1.5
ATM	Ataxia telangiectasia mutated (includes complementation groups A, C and D)	2.1	—
CRADD	CASP2 and RIPK1 domain containing adaptor with death domain	2.1	1.6
RIPK1	Receptor (TNFRSF)-interacting serine-threonine kinase-1	2.1	1.3
LTA	Lymphotoxin alpha (TNF superfamily, member-1)	−6.1	—
IL10	Interleukin-10	−4.4	—
TNFRSF8	Tumor necrosis factor receptor superfamily, member-8	−4.2	—
CCR4	Chemokine (C-C motif) receptor 4	−3.8	−2.6
IL2RA	Interleukin-2 receptor, alpha	−3.8	−2.6
TP53	Tumor protein p53 (Li-Fraumeni syndrome)	−3.5	−1.5
IKZF1	IKAROS family zinc finger-1 (Ikaros)	−3.4	−2.1
CCNB1	Cyclin B1	−3.3	−3.8
FAS	Fas (TNF receptor superfamily, member-6)	−3.3	−1.6
MKI67	Antigen identified by monoclonal antibody Ki-67	−3.2	−4.4
CDC2	Cell division cycle 2, G1 to S and G2 to M	−3.2	—
PLK1	Polo-like kinase 1 (Drosophila)	−3.0	−1.4
SULF1	Sulfatase 1	−3.0	—
BIRC5	Baculoviral IAP repeat-containing 5 (survivin)	−2.9	−3.8
CDK2AP1	CDK2-associated protein-1	−2.9	−1.1
AVEN	Apoptosis, caspase activation inhibitor	−2.8	—
MCM5	Minichromosome maintenance complex component-5	−2.8	−3.5
CDC25A	Cell division cycle 25 homolog A (*Schizosaccharomyces pombe*)	−2.7	−4.0
MYBL2	v-myb Myeloblastosis viral oncogene homolog (avian)-like-2	−2.7	−4.0
MYC	v-myc Myelocytomatosis viral oncogene homolog (avian)	−2.7	−1.9
BUB1B	BUB1 budding uninhibited by benzimidazoles 1 homolog beta (yeast)	−2.6	−4.1
CDCA3	Cell division cycle associated-3	−2.6	−3.5
FAIM	Fas apoptotic inhibitory molecule	−2.6	−2.1
ATF5	Activating transcription factor-5	−2.5	−3.3
WEE1	WEE1 homolog (*Schizosaccharomyces pombe*)	−2.5	−2.8
BCAT1	Branched chain aminotransferase 1, cytosolic	−2.4	−2.1
CCNA2	Cyclin A2	−2.4	−3.8
STEAP3	STEAP family member 3	−2.4	−1.3
ZAK	Sterile alpha motif and leucine zipper containing kinase AZK	−2.4	−3.2
CCNB2	Cyclin B2	−2.3	−3.8
FBXO5	F-box protein-5	−2.3	−2.6
HMGB1	High-mobility group box 1	−2.3	−2.7
NEK6	NIMA (never in mitosis gene a)-related kinase-6	−2.3	−3.2
RYR1	Ryanodine receptor 1 (skeletal)	−2.3	—
SFRS2	Splicing factor, arginine/serine-rich-2	−2.3	−1.7
AURKA	Aurora kinase A	−2.2	−3.0
BCLAF1	BCL2-associated transcription factor 1	−2.2	−1.9
CXCR4	Chemokine (C-X-C motif) receptor-4	−2.2	−1.7
E2F8	E2F transcription factor-8	−2.2	−3.4
CDC45L	CDC45 cell division cycle 45-like (S. cerevisiae)	−2.1	−4.3
CSE1L	CSE1 chromosome segregation 1-like (yeast)	−2.1	−1.8
HK2	Hexokinase-2	−2.1	—
NME1	Non-metastatic cells 1, protein (NM23A) expressed in	−2.1	−1.3

Abbreviation: TNF, tumor necrosis factor. HuT102 and LM-Y1 cells were treated with either vehicle or 50 nM of LBH589 for 24 h and DNA microarray analyses were performed. Among genes with changes in expression of at least 2.1-fold (log 2 ratio) in either direction in HuT102 cells, we picked those with known functions related to apoptosis, the cell cycle and cell proliferation.